Biological diversity of photosynthetic reaction centers and the solid-state photo-CIDNP effect

Roy, E.

3 Contrasting magnetic field dependence of ^{13}C photo-CIDNP MAS NMR in plant photosystems I and II

Photo-CIDNP is observed in the two photosynthetic reaction centers of plants, PSI and PSII by ^{13}C MAS NMR at three different magnetic fields, 17.6, 9.4 and 4.7 Tesla. There is a significant difference in field dependence detected in the light induced signal pattern of the two photosystems. For PSII the optimal NMR enhancement factor of ~5000 is observed at 4.7 Tesla. On the other hand, the strongest light induced signals of PSI are observed at 9.4 Tesla. Simulations indicate that this contrasting difference between the field dependence of PSI on one hand and purple bacterial RCs and PSII on the other hand is due to differences in the exchange coupling.

3.1 Introduction

Photosynthesis in plants involves the participation of two RCs, PSI and PSII, located in the thylakoid membrane of chloroplasts. The electron transfer chain of both photosystems has two symmetric branches consisting of six chlorin molecules and two quinones. PSI belongs to type-I RCs, characterized by three iron-sulphur clusters as the terminal intrinsic electron acceptors, while PSII belongs to the type-II RCs where a mobile quinone acts as the terminal electron acceptor. The primary donors of both RCs differ in their redox potential by ~700 mV (1). The oxidized electron donor of PSII, is the strongest oxidising agent known in living nature, having a redox potential of 1.2 V (2). In contrast, the electronically excited electron donor of PSI, is probably the most reducing compound in living nature (3). The coupling of these two photosystems facilitates the transfer of electrons across the photosynthetic membrane from water molecules finally into CO_2 in order to build up organic material. Despite their opposite functional roles, structural similarities in the arrangement of transmembrane helices in the cores of the two photosystems have been observed by recent structural data on PSI (4) and PSII (5).

Photo-CIDNP is well known in liquid NMR (6-8) as a method that increases NMR intensities. Strongly enhanced signals of solid samples upon continuous illumination with white light have been observed for the first time by applying ^{15}N MAS NMR to quinone-blocked bacterial RCs of *Rb. sphaeroides* R-26 (9, 10). ^{13}C photo-CIDNP MAS NMR experiments of R-26 (11-14) and WT (15-17) allow for the study of photochemically active

regions in great detail. In addition, photo-CIDNP has also been observed in both plant RCs. The ^{13}C photo-CIDNP MAS NMR signals obtained from the D1D2 complex of PSII provide evidence for a highly asymmetric electron spin density shifted towards the C-15 methine bridge on the donor chlorophyll (18). The ^{13}C photo-CIDNP MAS NMR data of the PSI complex show that all signals are emissive and can be assigned to a single Chl *a* molecule of the donor P700 (Chapter 2). Comparison between the two photosystems reveals that P700 is essentially an undisturbed Chl *a* cofactor, while the electronic structure of the P680 can be interpreted in terms of a monomeric Chl *a* cofactor having strong interaction with the protein matrix (19).

The mechanism of photo-CIDNP has recently been discussed extensively (14, 17, 20). In RCs of *Rb. sphaeroides* WT, photo-CIDNP has been explained as a combination of two mechanisms (17). The TSM mechanism is related to the dipolar and exchange couplings between two electron spins in a correlated radical pair state, leading to enhanced nuclear polarization via the anisotropic hyperfine coupling (21). The DD mechanism also requires anisotropic hyperfine coupling, to transfer the electron spin polarization to nuclear polarisation (22). However, in this case the build up of nuclear polarisation from the spin-correlated radical pair is due to the different lifetimes of the singlet and triplet states. On the other hand, in RCs of *Rb. sphaeroides* R-26, the carotenoid-less mutant, a third mechanism is involved due to the long lifetime of the donor triplet state (14). This DR mechanism is based on relaxation processes involving nuclear polarization on the triplet branch, while the nuclear polarization of the singlet branch survives entirely (23). These interpretations are in line with the magnetic field effects observed, showing NMR enhancement maxima of about 10,000 at 4.7 Tesla in both bacterial RCs (14, 17). Hence, magnetic field dependence of photo-CIDNP signals is a sensitive tool to study photo-CIDNP mechanisms and the linked magnetic parameters. In this chapter the field dependent ^{13}C photo-CIDNP MAS NMR data of plant PSI and PSII are presented.

3.2 Materials and Methods

3.2.1 *Sample Preparation*

PSI RC preparation. The PSI complex containing ~110 Chl/P700 was prepared from spinach (*Spinacia oleracea*) according to the method described in chapter 2. Briefly, the chloroplasts were isolated first, then washed with 10 mM Tricine buffer (pH 7.8) containing 50 mM Sorbitol and 5 mM EDTA, and subsequently re-suspended in buffer containing 10 mM Tricine (pH 7.8) to obtain a final concentration of 0.8 mg Chl/mL. The membranes (0.8 mg/mL) were solubilised with Triton X-100 (final concentration of 0.8% w/v) for 30 minutes at room temperature in the dark with continuous slow stirring. These solubilised membranes were loaded onto a linear sucrose gradient (0.1 - 1.0 M sucrose, 2 M sucrose cushion, 10 mM

Tricine, 0.02% Triton X-100, pH 7.8). PSI-110 particles appeared as a dark green non fluorescent band just above the 2 M sucrose. These particles were then dialysed and concentrated.

PSII RC preparation. PSII (D1D2-cytb559) from spinach (*Spinacia oleracea*) was isolated according to the method described in ref. (18). Briefly, PSII membrane fragments were isolated first and suspended in BTS200 [20 mM [bis(2-hydroxyethyl)amino] tris(hydroxymethyl) methane (Bistris), pH 6.5/20 mM $MgCl_2$/5 mM $CaCl_2$/10 mM $MgSO_4$/0.2 M sucrose/ 0.03% (wt/vol) *n*-dodecyl b-D-maltoside]. These membranes were further purified by removing the light harvesting complex and PSII core antenna proteins to obtain purified PSII RC complex, D1-D2-cytb559 with about 6 attached chlorophylls and 2 pheophytins. The RCs were concentrated for NMR measurements.

3.2.2 *MAS-NMR Measurements*

The NMR experiments were performed in different fields using AV-750, DMX-400 and DMX-200 NMR spectrometers (Bruker GmbH, Karlsruhe, Germany). The samples were loaded into optically transparent 4 mm sapphire rotors. The PSI sample was reduced by the addition of an aqueous solution of 10 mM sodium dithionite and 40 mM glycine buffer (pH 9.5) in an oxygen free atmosphere. Immediately following the reduction, slow freezing of the sample was performed directly in the NMR probe inside the magnet with liquid nitrogen-cooled gas under continuous illumination with white light. The PSII sample was also frozen slowly directly in the NMR probe inside the magnet with liquid nitrogen-cooled gas. The experiments have been performed at a temperature of 223 K, except for experiments at 9.4 Tesla, which were performed at a temperature of 240 K. The illumination set-up was specially designed for the Bruker MAS probe (12). The light and dark spectra were obtained with a Hahn echo pulse sequence and TPPM proton decoupling (24). Experimental line-broadening of 30 (at 4.7 Tesla), 70 (9.4 Tesla) and 120 Hz (17.6 Tesla) was applied. The number of scans was 20 k, unless stated differently.

3.2.3 *Calculations*

Numerical simulations of the field dependence of photo-CIDNP effects for PSI were based on the theory described in ref. (20) as implemented in a home-written Matlab program for density matrix computation using the EasySpin library (25). The program starts from a pure singlet state of the pair and computes time evolution for a Hamiltonian including electron Zeeman, nuclear Zeeman, and hyperfine interaction as well as dipole-dipole and exchange coupling between the two electron spins. Evolution is computed for a total time that exceeds the lifetime of both singlet and triplet pairs by a factor of five, so that radical pairs have completely decayed. The part of the density matrix that decays to the ground state from either singlet or triplet radical pairs is projected out. In this way the nuclear polarization of the

diamagnetic part of the density matrix is determined. This diamagnetic part is further evolved with a Hamiltonian including only the nuclear Zeeman interaction. As an extension to the approach described in ref. (20), this procedure is performed for a full powder average (17), describing all interactions by tensors, except for the nuclear Zeeman interaction since its anisotropy is negligible on a time scale of 100 ns. Powder averaging was performed using the EasySpin spherical grid function sphgrid with 16 knots and C_i symmetry. This yields 481 orientations. Nuclear polarization was normalized to the thermal polarization at the measurement temperature of 223 K and the given field.

Only few of the required spin Hamiltonian parameters for PSI RCs are known from experiments. The principal values for the *g* tensor of the primary donor cation radical, 2.00304, 2.00262, and 2.00220 were taken from ref. (25). To the best of our knowledge, no high-field EPR measurements of the *g* tensor have been reported, neither for the primary acceptor in PSI, which is believed to be a Chl *a* (26), nor for the Chl *a* anion radical. To obtain this missing *g* tensor, the orientations of the principal axes of both *g* tensors, and the ^{13}C hyperfine couplings, DFT computations based on the reported crystal structure of cyanobacterial PS1 have been performed (27). From the PDB structure 1JB0 the chlorophyll molecules CL2 1011 and CL1 1021 as the P700 donor and the chlorophyll molecule CL1 1013 as the putative primary acceptor were extracted. The amino acid residues that coordinate the Mg atoms of the chlorophyll molecules were also extracted, His A680 and His B660 for the P700 donor, and Met A688 for the acceptor. For the DFT computations, histidines were edited to methylimidazole molecules and methionine was edited to ethyl methyl thioether, and the phytyl chains of the chlorophyll molecules were replaced by methyl groups. Hydrogen atoms were added with the program Titan (Wavefunction, Inc., Irvine, CA, USA). In this procedure some sp^3 carbons were wrongly assigned as sp^2 carbons. These were edited by hand to sp^3 in the same program.

DFT computations were performed with the program ADF 2004.1 using the BLYP functional (28). The geometry of the P700 donor cation radical was optimized, using a double-zeta basis set and frozen cores up to 1s for C, N, and O atoms and up to 2p for the Mg atom. The *g* tensor was computed by a spin-restricted spin-orbit relativistic computation within the ZORA approach, using all-electron DZ basis sets for all atoms. Hyperfine couplings were obtained from a spin-unrestricted non-relativistic computation also using all-electron DZ basis sets. In attempts to optimize the geometry of the acceptor anion radical, it was found that the distance between the Mg atom of the chlorophyll and the coordinated S atom of the ethyl methyl thioester, which is 2.6 Å in the crystal structure (27), increased continuously. This may indicate that the unusual sulphur coordination to the magnesium is imposed by the structure of the protein and serves for fine tuning of the electron transfer chain, possibly by influencing the redox potential of the primary acceptor. For DFT

computations of magnetic parameters, the geometry as derived from the crystal structure without further optimization was used. The *g*-tensor of the acceptor anion radical was computed in the same way as for the P700 donor cation radical. While the principal axes directions were directly taken from the computation, the deviations of the principal values from the free electron *g* value were scaled by a factor *F* that gave the best agreement between experimental principal values and rescaled computed values for the BPhe acceptor in bacterial reaction centers. The principal values obtained by this procedure for the PSI acceptor (2.0039, 2.0030, 2.0024) are considered as rough estimates. Hyperfine couplings for the acceptor were obtained from a spin-unrestricted non-relativistic computation using all-electron TZ2P basis sets for all atoms.

The remaining parameters in the spin Hamiltonian, the exchange coupling and dipole-dipole coupling between the two electron spins, and the recombination rates of singlet and triplet radical pairs that influence the radical pair kinetics have not been determined exactly. Since the geometry and general electronic structure of the relevant part of the PSI RC are quite similar to bacterial RCs, it is assumed that the dipole-dipole coupling between the electron spins is rather close to the value determined on bacterial RCs (29). The average lifetime of the $P700^{+\bullet}$-$A_0^{-\bullet}$ radical pair of about 40 ns at zero magnetic field constrains the lifetimes of singlet and triplet pairs (30). These lifetimes, as well as the exchange coupling between the electron spins were varied in our photo-CIDNP simulations as described in the following sections.

3.2.4 *Calculation of the ratio of light induced signal to noise*

In order to compare the photo-CIDNP light induced signal intensity at the three different magnetic fields (17.6 Tesla, 9.4 Tesla and 4.7 Tesla) in PSI and PSII, the ratio of light-induced centerband signals relative to the noise has been determined. This ratio has been standardised to a single scan at different magnetic fields.

3.3 Results and Discussion

3.3.1 *Field effects in the dark and light spectra*

Fig. 3.1 shows the ^{13}C MAS NMR spectra of PSII particles at three different magnetic fields at 17.6 Tesla (750 MHz proton frequency), 9.4 Tesla (400 MHz) and 4.7 Tesla (200 MHz) recorded using a MAS rotational frequency of 8 kHz. All three dark spectra show similar features. Strong signals appear between 110 and 10 ppm, with a weaker response in the aromatic and carbonylic region. The spectra show the characteristic features of ^{13}C MAS NMR spectra of large proteins (31). No spinning sidebands are observed in the three spectra. This is due to the small CSA of aliphatic carbons and the weak signal intensity of the carbonylic and aromatic signals. The spectral quality obtained at 17.6 Tesla is slightly better

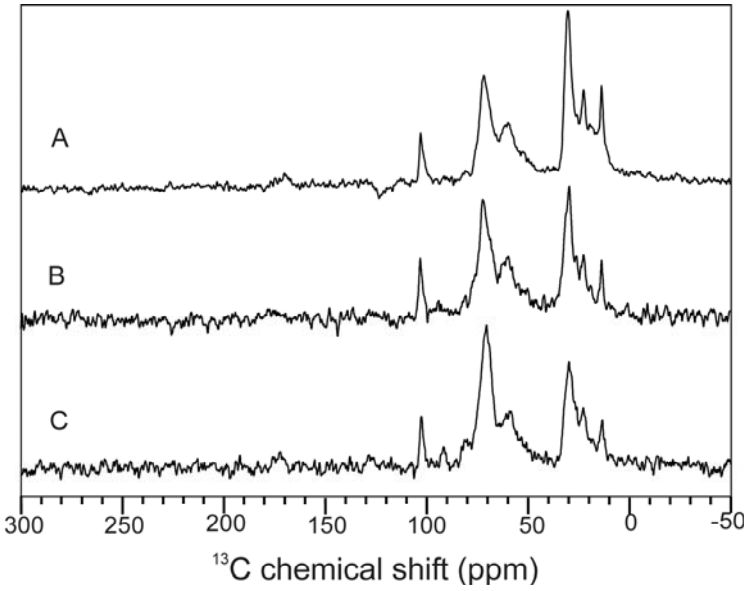

Figure 3.1. ^{13}C MAS NMR spectra of PSII particles obtained in the dark at a MAS frequency of 8 kHz at (A) 17.6, (B) 9.4, and (C) 4.7 Tesla.

than that obtained at 9.4 Tesla. Both Spectra 3.1A and 3.1B are slightly better resolved than Spectrum 3.1C, obtained at 4.7 Tesla. The observed field dependence is due to less Zeeman spitting and chemical shift dispersion at lower fields under Boltzmann conditions.

The ^{13}C MAS NMR spectra of PSI samples at three different magnetic fields at 17.6 Tesla, 9.4 Tesla and 4.7 Tesla recorded using MAS rotational frequency of 8 kHz did not show a significant signal of the protein backbone (data not shown). This is due to the presence of a small amount of protein, which was estimated to be 0.6 mg, present in the rotor, while the amount of protein in the rotor for PSII sample has been determined to be 15.8 mg.

Upon illumination with continuous white light, strong signals emerge in the aromatic region in both, PSI (Fig. 3.2) and for PSII (Fig. 3.3). In PSI, all light induced signals appear to be emissive (negative) between 170 and 80 ppm (19). In the spectrum at 17.6 Tesla (Fig 3.2A), spinning sidebands can be observed, while at lower fields the entire intensity is concentrated in the centerband. The strongest signals are observed at 9.4 Tesla (Fig 3.2B), while the weakest signals are observed at 4.7 Tesla (Fig 3.2C). Table 3.1 expresses the field-dependence of the light-induced centerband signals relative to the noise standardized to a single scan. The table shows a maximum at 9.4 T and about half the intensity at 17.6 Tesla for PSI.

In PSII, strong enhancement is observed at 4.7 and 9.4 Tesla (Fig. 3.3B and C), while at 17.6 Tesla (Fig. 3.3A) the light induced signals are negligible. Comparing Fig 3.3B and C indicates a slightly stronger enhancement compared to the dark signals at 4.7 Tesla. In contrast to the light-induced signals in PSI, both enhanced absorptive and emissive light-

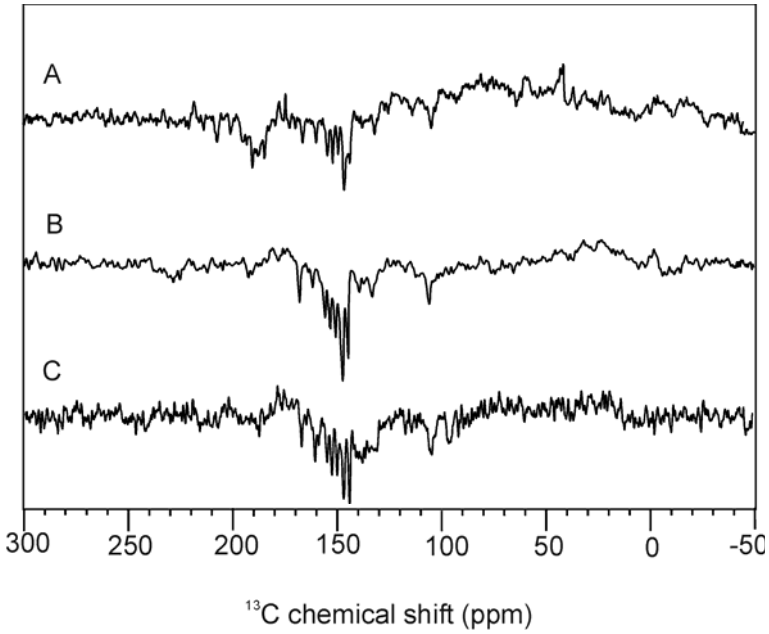

Figure 3.2.^{13}C MAS NMR spectra of PSI particles obtained under continuous illumination with white light at a MAS frequency of 8 kHz at (A) 17.6 Tesla, (B) 9.4 Tesla, and (C) 4.7 Tesla.

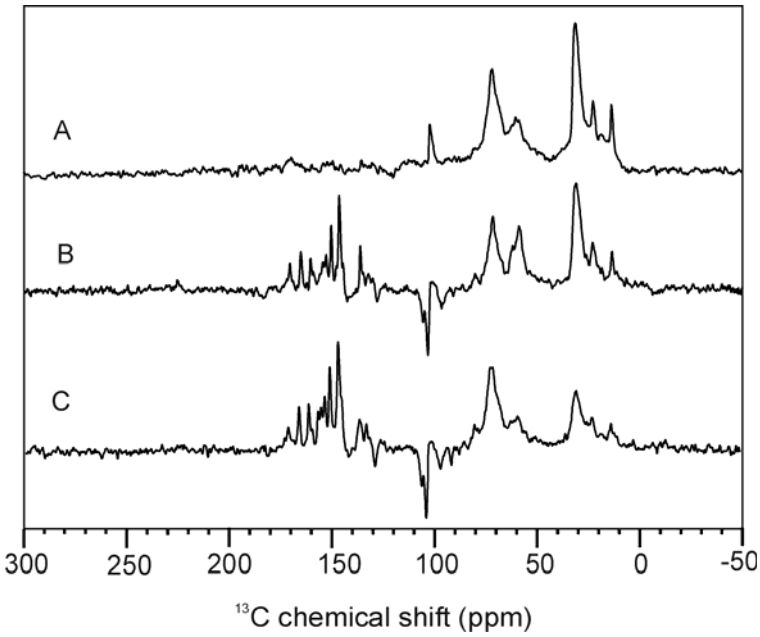

Figure 3.3. ^{13}C MAS NMR spectra of PSII (D1D2) particles obtained under continuous illumination with white light at a MAS frequency of 8 kHz at (A) 17.6 Tesla, (B) 9.4 Tesla, and (C) 4.7 Tesla.

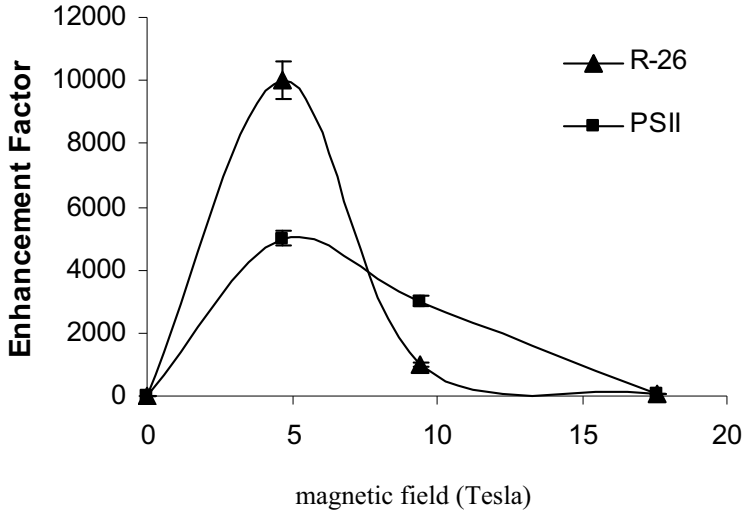

Figure 3.4. Enhancement factors at different magnetic fields calculated for PSII along with R-26. The assumption of an enhancement factor of zero at zero magnetic field is discussed in ref. 20.

induced signals occur.

The emissive signals mainly appear in the region of the methine carbons. In the spectrum at 9.4 T, weak spinning sidebands can be observed. The enhancement factor has been calculated as a ratio of the signal due to a single carbon at 147.3 ppm (positive signal) and 105 ppm (negative signal) to one at 13.7 ppm (in the dark) in the case of PSII. Using the signal from about 900 methyl groups of the entire D1D2 complex at 13.7 ppm as an internal standard, enhancement factors of ≤60 (17.6 Tesla), 3000 (9.4 Tesla) and about 5000 (4.7 Tesla) were calculated for PSII (Fig. 3.4). The enhancement factor for PSI could not be calculated due to absence of reliable dark signals.

The field-dependence of the enhancement factor of PSII is similar to that observed in bacterial RCs of both WT and R-26 (14, 17), showing a maximum at 4.7 Tesla and a strong decay for higher fields. The field-dependence of the ratio between the light induced signal to the standardized noise is shown in Table 3.1, allowing for comparison with PSI suggesting a shift of optimum photo-CIDNP production in PSI to higher fields.

Magnetic field	PSI	PSII
Tesla	S_{Li} / N_{st}	S_{Li} / N_{st}
4.7	2.0	9.4
9.4	10.7	10.0
17.6	4.3	0

Table 3.1. The field-dependence of the ratio of light-induced signal (S_{Li}) to the standardized noise (N_{st}) for PSI and PSII.

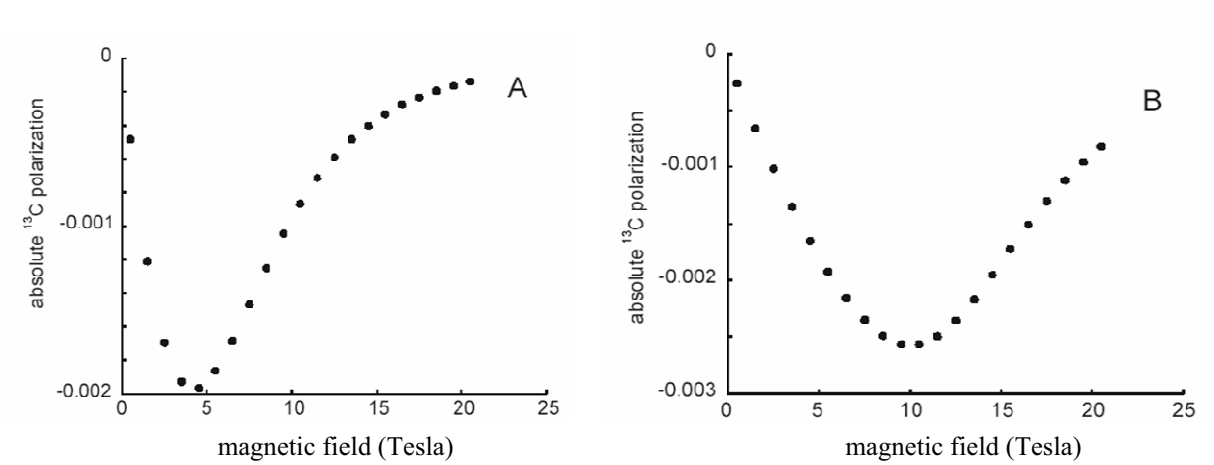

Figure 3.5. Simulated field dependence of the absolute ^{13}C polarization for the methine carbon C-20 of branch B of P700 donor. Similar results are obtained for other carbon atoms in both donor and acceptor. (A) Radical pair lifetimes and exchange coupling as in bacterial RCs. (B) Radical pair lifetime as in bacterial RCs, but exchange coupling increased by a factor of three.

3.3.2 *Simulations of field effects in light spectra of PSI*

The field dependence of the photo-CIDNP effects in PSII is similar to previous observations on bacterial RCs, with maximum polarization at the lowest tested field of 4.7 Tesla (Fig. 3.4). In contrast, PSI exhibits only a relatively weak photo-CIDNP effect at 4.7 Tesla and a significantly stronger polarization at 9.4 Tesla (Fig. 3.2, Table 3.1). As the field dependence of the nuclear polarization is related to the magnetic parameters and lifetimes of the intermediate radical species (17, 20), this difference reflects a difference in the electronic structure between RCs of purple bacteria on the one hand and PSII and PSI RCs on the other hand. To examine what parameter changes can explain the experimental observations simulations were performed of photo-CIDNP in an analogous manner as the simulations of bacterial RCs, which reproduced the experimental field dependence (17). Generally, the field dependence of the nuclear polarization appears similar for all ^{13}C nuclei in both donor and acceptor molecules, as was also found for the bacterial RCs.

The simulation is in line with the experimental observation that the spectral pattern varies only slightly between 4.7 and 17.6 Tesla (Fig. 3.1). In addition, it is found that any reasonable changes in the *g*-tensors (up to ±50% of the deviation from the free electron *g*-value) cause only a scaling of the intensity of the whole spectral pattern by a constant factor, which does not depend significantly on the magnetic field. In other words, uncertainties in the computation of the acceptor *g*-tensor and of the principal axes directions of the *g*-tensors do not lead to significant uncertainties in the computed field dependence of the nuclear polarization. Likewise, any reasonable changes in the dipole-dipole coupling, up to ±30% of the coupling strength, have little effect on the field dependence. This suggests that the pronounced difference between bacterial and PSII RCs on the one hand and PSI RCs on the

other hand can thus be traced back to either a difference in radical pair lifetimes or a difference in the exchange coupling *J*.

Assuming the same *J* and lifetimes as for bacterial RCs, we calculate a very similar field dependence of the nuclear polarization with a maximum close to 5 Tesla. As an example, the dependence for the methine carbon C-20 of the donor for these assumptions is shown in Fig. 3.5A. First it was tested whether the different field dependence observed for PSI RCs can be reproduced by changing the ratio between the lifetime T_S of radical pairs in the singlet state and the lifetime T_T of radical pairs in the triplet state. However, changes in the field dependence of the nuclear polarization are minor when varying the ratio T_S/T_T between 0.5 and 50 (data not shown).

Next, it was tested whether changes in the mean lifetime of radical pairs, defined here as $\sqrt{T_S T_T}$, can reproduce the observations. Indeed the shift of the maximum to a field of approximately 8.5 T can be obtained by decreasing $\sqrt{T_S T_T}$ to 1.6 ns (data not shown). This value cannot directly be compared to the experimental lifetime, as the combination of the lifetimes T_S and T_T to the true mean lifetime depends on the specifics of spin evolution and would have to be computed by including hyperfine coupled protons in the spin Hamiltonian. However, the mean lifetime cannot be larger than the maximum of T_S and T_T, which is 5 ns for simulations that fit the observed field dependence. It seems unlikely that the radical pair lifetime in our samples is by almost a factor of ten shorter than found on cyanobacterial PSI (30). Even if this was to be assumed, still the fact that such a shortening of the lifetime leads to a drastic decrease in the absolute nuclear polarization remains, which does not agree with the similar NMR sensitivity observed in photo-CIDNP experiments on bacterial RCs and plant PSI RCs. Thus a shortening of the radical pair lifetime as the cause for the change in the field dependence is excluded.

Finally, variations of the exchange coupling *J* are considered. An increase of the exchange coupling by a factor of three compared to bacterial RCs to 21G shifts the field where maximum nuclear polarization is attained to about 10 T (Fig. 3.6B). This leads to a slight increase in absolute polarization, which can be reconciled with experimental observations. Such a change in *J* may well be caused by slight rearrangements of the cofactors that lead to an improved overlap between the molecular orbitals of the P700 donor and the accessory Chl *a* or between the molecular orbitals of the accessory chlorophyll and the primary acceptor A_0. The simulations thus indicate that the change in the magnetic field dependence of solid-state photo-CIDNP between bacterial RCs and plant PSI can be traced back to an increase of the exchange coupling between the $P700^{+\bullet}$ and $A_0^{-\bullet}$ radical anions by a factor of approximately three. The underlying cause for this change is the influence of a large exchange coupling on the matching condition (20). In the limit where the exchange coupling is much larger than the hyperfine couplings and the difference of the electron Zeeman frequencies, state mixing is

optimal when the coupling between the electron spins matches the nuclear Zeeman frequency. In the limit of large exchange couplings the optimum magnetic field is thus proportional to the exchange coupling.

References

1. Grotjohann, I.; Jolley, C.; Fromme, P., *Phys. Chem. Chem. Phys.* **2004**, 6, 4743-4753.
2. van Gorkom, H.J.; Schelvis, J.P.M., *Photosynth. Res.* **1993**, 38, 297-301.
3. Webber A.N.; Lubitz W., *Biochim. Biophys. Acta* **2001**, 1507, 61-79.
4. Jordan P.; Fromme P.; Witt H.T.; Klukas O.; Saenger W.; Krauss N., *Nature* **2001**, 411, 909-917.
5. Zouni A.; Witt H.T.; Kern J.; Fromme P.; Krauss N.; Saenger W.; Orth P., *Nature* **2001**, 409, 739-743.
6. Roth, H.D. In *Encyclopaedia of Nuclear Magnetic Resonance*. Wiley: Chichester, U.K., 1996; p 1337-1350.
7. Hore, P.J.; Broadhurst, R.W., *Prog. Nucl. Magn. Reson. Spectrosc.* **1993,** 25, 345-402.
8. Goez, M., A*dv .Photochem.* **1997**, 23, 63-164.
9. Zysmilich M.G.; McDermott A., *J. Am. Chem. Soc.* **1994**, 116, 8362-8363.
10. Zysmilich M.G.; McDermott A., *J. Am. Chem. Soc.* **1996**, 118, 5867-5873.
11. Zysmilich, M.G.; McDermott, A., *Proc. Natl. Acad. Sci. U. S. A.* **1996**, 93, 6857-6860.
12. Matysik, J.; Alia; Hollander, J.G.; Egorova-Zachernyuk, T.; Gast, P.; de Groot, H.J.M., *Indian J. Biochem. Biophys.* **2000**, 37, 418-423.
13. Matysik, J.; Alia; Gast, P.; Lugtenburg, J.; Hoff, A.J.; de Groot, H.J.M. In *Perspectives on solid state NMR in biology*; Kiihne, S., de Groot H.J.M., Eds.; Kluwer: Dordrecht, 2001; p 215-225.
14. Prakash, S.; Alia; Gast, P.; de Groot, H.J.M.; Matysik, J.; Jeschke, G., *J. Am. Chem. Soc.* **2006**, 128, 12794-12799.
15. Schulten, E.A.M.; Matysik, J.; Alia; Kiihne, S.; Raap, J.; Lugtenburg, J.; Gast, P.; Hoff, A.J.; de Groot, H.J.M., *Biochemistry* **2002**, 41, 8708-8717.
16. Prakash, S.; Alia; Gast, P.; Jeschke, G.; de Groot, H.J.M.; Matysik, J., *J. Mol. Struct.* **2003**, 661, 625-633.
17. Prakash, S.; Alia; Gast, P.; de Groot, H.J.M.; Jeschke, G.; Matysik, J., *J. Am. Chem. Soc.* **2005**, 127, 14290-14298.
18. Matysik, J.; Alia; Gast, P.; van Gorkom, H.J.; Hoff, A.J.; de Groot, H.J.M., *Proc. Natl. Acad. Sci. U. S. A.* **2000**, 97, 9865-9870.
19. Diller A.; Alia; Roy E.; Gast P.; van Gorkom H.J.; Zaanen J.; de Groot H.J.M.; Glaubitz C.; Matysik J., *Photosynth. Res.* **2005**, 84, 303-308.
20. Jeschke, G.; Matysik, J., *Chem. Phys*. **2003**, 294, 239-255.
21. Jeschke G., *J. Chem. Phys*. **1997**, 106, 10072-10086.
22. Polenova T.; McDermott A.E., *J. Phys. Chem. B* **1999**, 103, 535-548.
23. McDermott A.; Zysmilich M.G.; Polenova T., *Solid State Nucl. Magn. Reson.* **1998**, 11, 21-47.
24. Bennett A.E.; Rienstra C.M.; Auger M.; Lakshmi K.V.; Griffin R.G., *J. Chem. Phys.* **1995**, 103, 6951-6958.
25. Stoll, S.; Schweiger, A., *J. Magn. Reson*. **2006**, 178, 42-55.
26. Petrenko, A.; Maniero, A.L.; Van Tol, J.; MacMillan, F.; Li, Y.; Brunel, L.-C.; Redding, K., *Biochemistry* **2004**, 43, 1781-1786.
27. Jordan, P.; Fromme, P.; Witt, H.T.; Klukas, O.; Saenger, W.; Krauss, N., *Nature* **2001**, 411, 909-917.

28. Velde, G.T.; Bickelhaupt, F.M.; Baerends, E.J.; Guerra, C.F.; van Gisbergen, S.J.A.; Snijders, J.G.; Ziegler, T., *J. Comput. Chem.* **2001**, 22, 931-967.
29. Hulsebosch, R.J.; Borovykh, I.V.; Paschenko, S.V.; Gast, P.; Hoff, A.J., *J. Phys. Chem. B* **1999**, 103, 6815-6823.
30. Biggins, J.; Mathis, P., *Biochemistry* **1988**, 27, 1494-1500.
31. Castellani, F.; van Rossum, B.; Diehl, A.; Schubert, M.; Rehbein, K.; Oschkinat, H., *Nature* **2002**, 420, 98-102.